Zeng *et al. Microstructures* **2025**, *5*, 2025010
DOI: 10.20517/microstructures.2024.2

Microstructures

Research Article

Open Access

Check for updates

Ti-Zr-V-Nb-Al BCC high-entropy alloy with outstanding uniform ductility achieved by grain refinement

Hanlin Zeng[1,#], Mengyunqing Han[1,#], Bolun Li[4], Liang Wang[1], Ke Jin[1,3], Benpeng Wang[1,2], Shihai Sun[1,2], Lu Wang[1], Yunfei Xue[1,2]

[1]School of Materials Science and Engineering, Beijing Institute of Technology, Beijing 100081, China.
[2]Tangshan Research Institute, BIT, Tangshan 063000, Hebei, China.
[3]Advance Research Institute of Multidisciplinary Sciences, Beijing Institute of Technology, Beijing 100081, China.
[4]Chongqing Hongyu Precision Industrial Co., Ltd, Chongqing 402760, China.
#Authors contributed equally.

Correspondence to: Dr. Benpeng Wang, School of Materials Science and Engineering, Beijing Institute of Technology, Haidian District, Beijing, China. E-mail: wangbenpeng@bit.edu.cn; Prof. Yunfei Xue, School of Materials Science and Engineering, Beijing Institute of Technology, Haidian District, Beijing, China. E-mail: xueyunfei@bit.edu.cn

How to cite this article: Zeng, H.; Han, M.; Li, B.; Wang, L.; Jin, K.; Wang, B.; Sun, S.; Wang, L.; Xue, Y. Ti-Zr-V-Nb-Al BCC high-entropy alloy with outstanding uniform ductility achieved by grain refinement. *Microstructures* **2025**, *5*, 2025010. https://dx.doi.org/10.20517/microstructures.2024.2

Received: 9 Jan 2024 **First Decision:** 8 Feb 2024 **Revised:** 20 Feb 2024 **Accepted:** 18 Mar 2024 **Published:** 25 Jan 2025

Academic Editor: Huijun Li **Copy Editor:** Ping Zhang **Production Editor:** Ping Zhang

Abstract

The lack of sufficient uniform deformation ability of body-centered cubic (BCC) high-entropy alloys (HEAs) is the obstacle to their applications as structural materials. Here we present a grain refinement strategy to achieve excellent uniform ductility of a BCC non-equal atomic ratio Ti-Zr-V-Nb-Al (TZ) alloy. The uniform elongation and yield strength of the fine-grained TZ alloy with a grain size of 15 μm are as high as ~12% and 840 MPa, respectively. The outstanding uniform deformability of the fine-grained TZ alloys is due to the frequent cross-slip events and abundant dislocation tangles. Grain refinement can increase the probability of dislocation entanglement, thereby promoting a rise in the work-hardening rate. The good plasticity and high work-hardening rate can improve the uniform deformation ability. Our results will give new insights into enhancing uniform ductility while maintaining high strength in the BCC HEAs.

Keywords: High-entropy alloys, grain refinement, dislocation density, uniform deformation

INTRODUCTION

Recently, high-entropy alloys (HEAs) have garnered significant attention due to their unique composition design concept and potential performance advantages[1-5]. Refractory body-centered cubic (BCC) structured HEAs usually have intrinsic high strength but poor work-hardening ability, such as TiZrNb and VNbTiTa alloys[6-10].

Previously reported BCC HEAs show that typical long planar-slip bands can be generated at the early plastic deformation stage[11-13]. Dislocations usually gather in these narrow planar-slip bands, leading to severe deformation localization. The grain boundary is a common obstacle that offers resistance to dislocation movement[14], which can effectively impede the long-range propagation of the planar-slip bands. Increasing the number of grain boundaries is expected to improve the possibility of dislocation entanglement near grain boundaries during alloy deformation. As a large number of dislocations become continuously entangled near the grain boundaries, the strengthening of the grain boundaries becomes more and more significant. Therefore, the grain refinement strategy is expected to improve the work-hardening ability of BCC HEAs. Meanwhile, grain boundaries can act as a source of dislocations[15,16]. More uniformly distributed grain boundaries lead to homogeneous dislocation nucleation, which improves the plastic deformation of the alloy. The high work-hardening ability and good plasticity are expected to promote uniform deformation ability. In addition, grain refinement is beneficial to improve alloy strength, which has been proved in many HEAs, such as AlFeCoNiCu, AlCrFeCoNiNb and AlTiFeCoNi[1,2,4].

The increase in grain boundaries ensures a uniform distribution of dislocations, effectively avoiding stress concentration and enhancing the ability for uniform deformation. On this basis, a simple fine-grain strategy was used to improve the uniform ductility of BCC HEAs. We have designed lightweight HEAs Ti-Zr-V-Nb-Al (TZ) alloys with high specific strength. However, these alloys exhibit almost no work-hardening ability resulting in limited engineering application. Here we present a grain refinement strategy to improve uniform ductility[11]. The effect of grain refinement on the uniform plasticity of TZ alloys was discussed in detail.

EXPERIMENTAL PROCEDURE

The theoretical atomic ratio composition of TZ alloy is: $Ti_{50}Zr_{18}Nb_{15}V_{12}Al_5$. Ti, Zr, V, Nb, and Al (purity > 99.9 wt%) with specified compositions were arc melted in an argon environment to create all TZ alloys. To get uniform ingots, the alloy ingots were remelted five times. The as-cast alloy was homogenized at 1,000 °C for 1 h followed by water quenching. Homogenized samples were cut into plates with 30 × 10 × 10 mm^3. The samples were cold-rolled to a thickness reduction of 70% and carried out a recrystallization treatment at 700 °C for 30 min, followed by water quenching.

The crystal structure of the alloy was characterized by the high energy X-ray diffraction (HEXRD) technology at the 11-ID-C beamline of the Advanced Photon Source at Argonne National Laboratory, USA. The X-ray wavelength was ~0.1173Å, and the beam size was 500 × 500 μm^2. The 2D diffraction patterns were collected using a Perkin-Elmer detector. The distances from samples to detectors are ~1,700 mm. Fit2D and GSAS-II software packages were used to get the X-ray diffraction (XRD) data[17].

The room-temperature tension tests were evaluated using a CMT4105 universal electronic tensile testing machine at the strain rate of 1×10^{-3} s^{-1}. The gauge part of each dog-bone shape tensile specimen is 1 × 3 × 10 mm^3. The *in-situ* tensile experiments were conducted on the TZ alloys utilizing the synchrotron-based HEXRD technique, with a strain rate of 1×10^{-3} s^{-1}.

The microstructure of the alloy was investigated using JEOL JSM-7001F scanning electron microscopy (SEM, the voltage is 15 kV and the current is 12 A) with an electron backscatter diffraction (EBSD) prober; the step size of EBSD testing varies depending on the selected area, ensuring a resolution of ≥ 500 px at all times. Microstructure and crystal structure characterization were performed using an FEI Tecnai F20 transmission electron microscope (TEM) at a working voltage of 200 kV. The TEM samples were thinned to 40-60 μm by 400-6,000 grit SiC papers and subsequently prepared by twin-jet electro-polishing at -15 °C in an electrolyte consisting of a volume of 6% perchloric acid, 35% butanol and 59% water.

RESULTS AND DISCUSSION

The grain size of the TZ alloys after homogenization heat treatment [Figure 1A] and after recrystallization treatment [Figure 1B] was characterized by EBSD analysis. According to the statistics, the average grain size of the coarse-grained and fine-grained TZ alloys is ~160 μm and ~15 μm, respectively. The phase constitution of the TZ alloy was characterized by HEXRD. Figure 2 shows the HEXRD results, which reveal diffraction peaks corresponding to single-phase BCC structure.

The tensile mechanical properties of the fine- and coarse-grained TZ alloys are displayed in Figure 3. The yield strength and elongation-to-failure of the coarse-grained TZ alloy are 790 MPa and 20%, respectively, while those of the fine-grained TZ alloy are 840 MPa and 25%, respectively. After the grain refinement strategy, the strength and ductility of TZ alloys have been improved. Three parallel specimens were tested to ensure the repeatability. The tensile properties of fine- and coarse-grained TZ alloys with the standard deviations were shown in Table 1.

The strain-hardening rates of the coarse- and fine-grained TZ alloys are shown in Figure 4. The necking point is the intersection point between the work-hardening rate curve and the true stress-strain curve, and the strain of the yield point is uniform elongation. Coarse-grained TZ alloys demonstrate almost no work-hardening ability, with a uniform elongation of about 2%. The fine-grained TZ alloy exhibits a strain-hardening rate of about 1100 MPa and a normalized strain-hardening rate of approximately 1.15, which is higher than most other reported BCC alloys, where the value is typically below 1[6,13]. The higher normalized strain-hardening rate results in a higher uniform elongation for the fine-grained TZ alloys[18]. Therefore, the alloy achieves a considerable uniform elongation of about 12%, which is excellent compared to other reported BCC HEAs[19].

The movement of dislocations governs the mechanical behavior of alloys to a large extent. The multiplication of dislocation significantly influences the uniform ductility of the alloy. Further in situ synchrotron HEXRD experiments were conducted to investigate dislocation density during deformation in coarse- and fine-grained TZ alloys. The modified Williamson-Hall method is used to quantify the variation in dislocation density during the tensile process, which is expressed as[20,21].

$$\Delta K = \frac{0.9}{d} + \left(\frac{\pi M^2 b^2}{2}\right)^{1/2} \rho^{1/2} \left(K\overline{C}^{1/2}\right) \quad (1)$$

Where $\Delta K = \frac{2\Delta\theta\cos\theta}{\lambda}$; $K = \frac{2\sin\theta}{\lambda}$; θ is the Bragg angle, Δθ is half of the full width at half maximum, d is the grain size, and M is a dimensionless constant value depending on the effective outer cut-off radius of dislocations. b is the Burgers vector module, ρ is the dislocation density and $\overline{C}$ is the dislocation contrast factor, which is influenced by the line vectors of dislocations, the diffraction vector, and anisotropic elastic constants[22]. From the linear fit of the modified Williamson-Hall plot, the slope m was calculated and dislocation density ρ was obtained from the relation $\rho = \frac{2m^2}{\pi M^2 b^2}$.

Table 1. The tensile properties of fine- and coarse-grained TZ alloys

Sample	Tensile yield strength (MPa)	Elongation (%)
Fine-grained TZ alloy	840 ± 7	25 ± 1
Coarse-grained TZ alloy	790 ± 8.5	20 ± 1.2

TZ: Ti-Zr-V-Nb-Al.

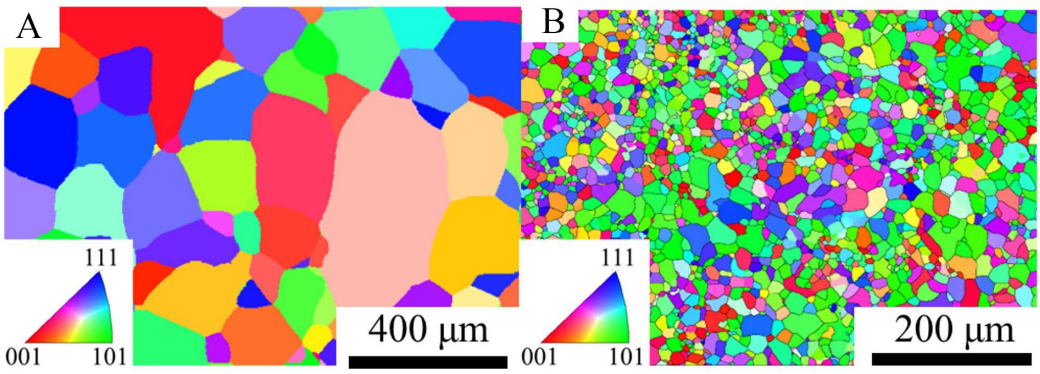

Figure 1. EBSD image of the TZ alloys after homogenization heat treatment (A) and after recrystallization treatment (B). EBSD: Electron backscatter diffraction; TZ: Ti-Zr-V-Nb-Al.

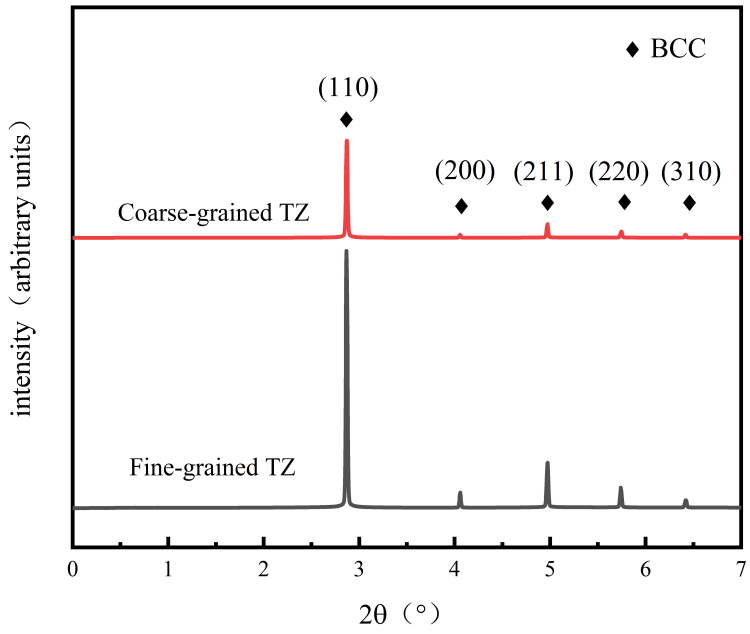

Figure 2. HEXRD pattern of coarse- and fine-grained TZ alloys. TZ: Ti-Zr-V-Nb-Al; HEXRD: High energy X-ray diffraction.

The *in-situ* tensile experiments were conducted with strains of 1%, 3%, 5%, 7%, 9%, and 12%. The selected calculation area for dislocation density (1, 2, 3, 4, 5, 6) of the specimen is marked in Figure 5A. Figure 5B and C show the evolution of the dislocation density in coarse-grained and fine-grained TZ alloys, respectively. As deformation increases, atoms in the crystal slip, forming dislocations. As the load rises, dislocation motion occurs, and the interaction between dislocations promotes the creation of new dislocations, resulting in a higher dislocation density. In Figure 5B, after 3% strain of the coarse-grained TZ

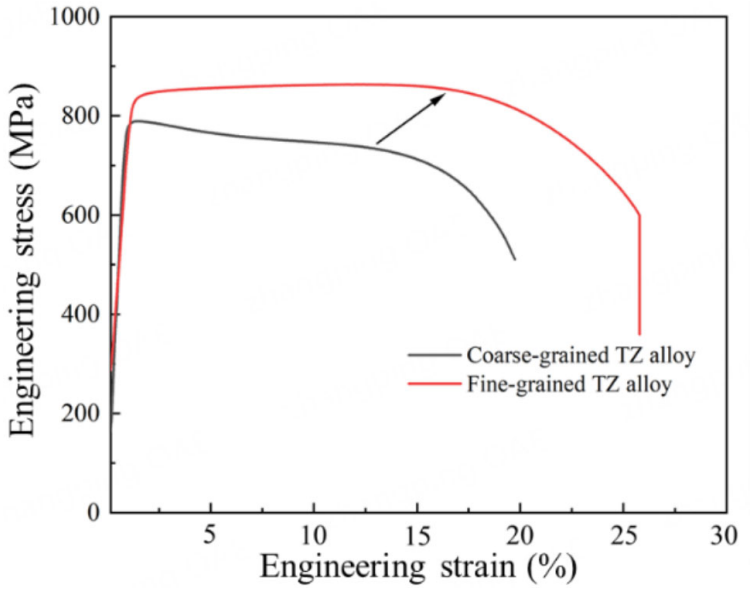

Figure 3. The tensile engineering stress-strain curves of coarse- and fine-grained TZ alloys. TZ: Ti-Zr-V-Nb-Al.

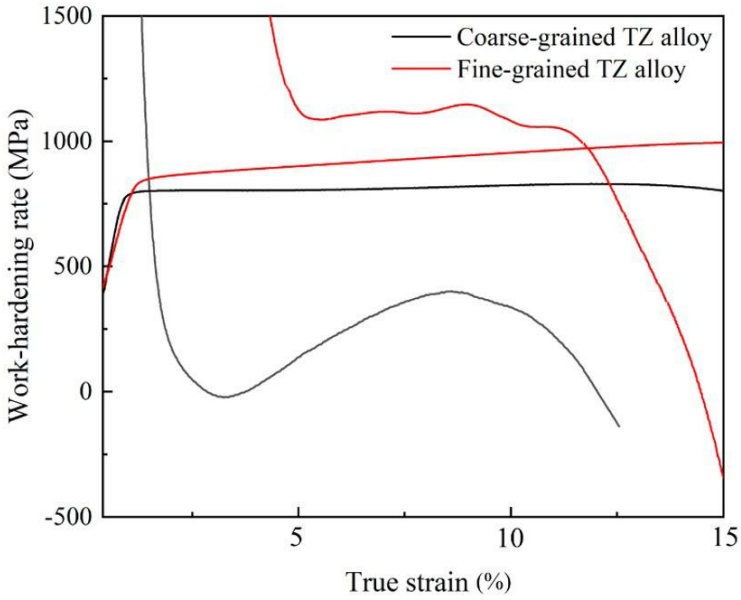

Figure 4. The strain-hardening rate and stress-strain curve of coarse- and fine-grained TZ alloys. TZ: Ti-Zr-V-Nb-Al.

alloy, dislocation density at positions (2, 3, 4, 5) increases sharply, while the dislocation density at positions 1 and 6 remains almost unchanged. This phenomenon is related to the occurrence of necking and a significant increase in deformation. As shown in Figure 5C, until a strain of 9%, the growth rate of dislocation density in each position of the fine-grained TZ alloy is consistent. The dislocation density distribution of the alloy is very uniform up to 12% strain. Compared to the coarse-grained TZ alloy, the grain refinement strategy delays the onset of necking and improves the uniform deformation ability of the TZ alloy.

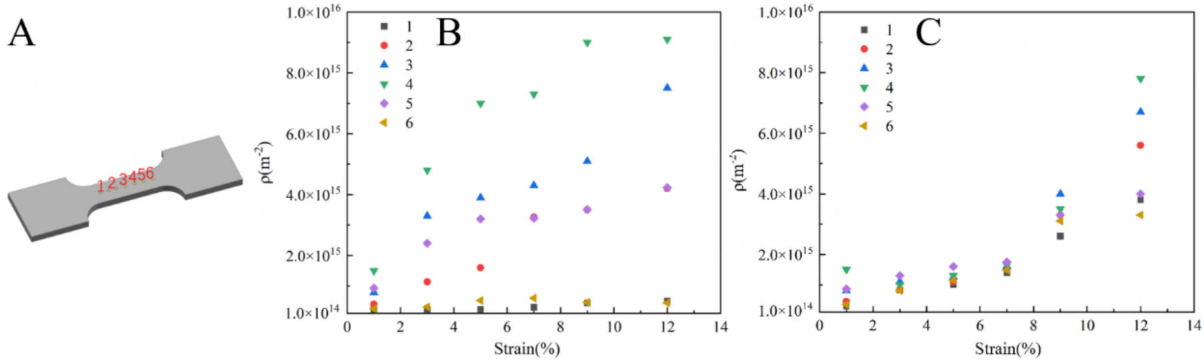

Figure 5. Schematic diagram of the chosen different locations (A); the dislocation density at chosen locations at 1%, 3%, 5%, 7%, 9% and 12% strains of coarse- (B) and fine-grained (C) TZ alloys. TZ: Ti-Zr-V-Nb-Al.

To clarify the deformation mechanism in the fine-grained TZ alloy, the deformed microstructure with 5% strain was analyzed. Figure 6A-C shows TEM images taken along the [111] axis. As seen in Figure 6A, planar-slip bands of different directions intersect, showing extensively networked dislocation patterns. Figure 6B shows dislocation structures within grains, where the planar-slip bands away from the grain boundaries are straight and sparse, while the dislocations close to grain boundaries become denser and entangle with each other in [Figure 6C]. Grain boundaries not only serve as dislocation sources but also impede dislocation motion[15,16]. When dislocations slip to the grain boundaries, their motion is halted, and numerous new dislocations are generated nearby. The fine-grained TZ alloy exhibits a pronounced propensity for dislocation to accumulate at grain boundaries. Therefore, increasing the grain boundary density of the alloy promotes a more uniform distribution of dislocations, as shown in Figure 6D, enhancing the alloy's ability to deform uniformly.

Figure 7 shows slip band morphologies among the fine-grained TZ alloy formed during deformation. At low tensile strain [Figure 7A], numerous long slip bands indicate that planar slip is the dominant deformation mode, with grain boundaries preventing the formation of continuous slip bands. At 5% strain, wavy slip lines are clearly seen in Figure 7B, suggesting dislocation cross-slip[23]. Multiple slips and enhanced dislocation interactions are beneficial to strain hardening. As shown in Figure 7C, there are much denser wavy slip lines formed at 9% strain, indicating frequent cross-slip events, which improve the plastic deformation capacity[24]. The average spacing d_s of the slip line is measured, with slip line density defined as $1/d_s$, as shown in Figure 7D. The grain boundary is determined as the base point, with the region within a quarter of the grain diameter defined as "close to the grain boundary", and the area beyond that as "far from the grain boundary". Slip lines near the grain boundaries are denser than those farther away. Grain boundaries impede dislocation motion and promote the activation of more slip lines, avoiding stress concentrations.

Figure 8 shows the specific yield strength *vs.* uniform elongation of the TZ alloy and several previously reported BCC HEAs. The fine-grained TZ alloy exhibits a superior combination of high specific strength (152 MPa*cm^3/g) and large uniform elongation (12.0%). Remarkably, the TZ alloy demonstrates higher uniform ductility compared to other BCC HEAs. The outstanding uniform deformability of the fine-grained TZ alloys is attributed to frequent cross-slip events and abundant dislocation tangles. These findings provide new insights into enhancing uniform ductility while maintaining high strength in BCC HEAs.

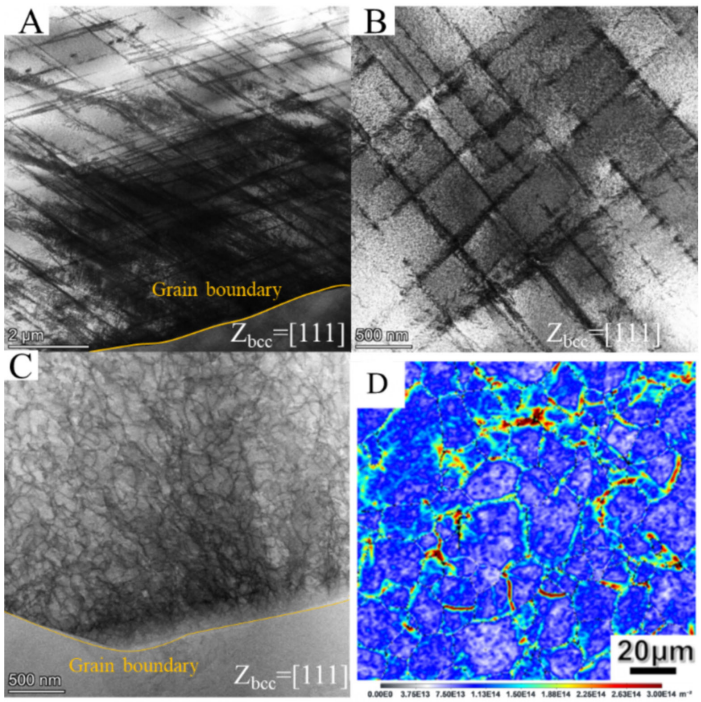

Figure 6. At 5% strain, the bright-field transmission electron microscopy (BF-TEM) observation of the dislocation (A-C) and GND density map (D) where the resolved region is selected from the necking region of fine-grained TZ alloy. TZ: Ti-Zr-V-Nb-Al; GND: Geometric necessary dislocation.

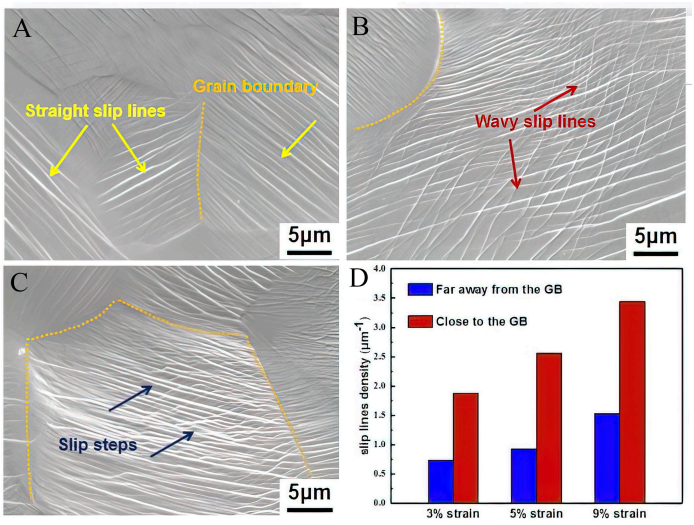

Figure 7. SEM image of the TZ at 3% (A); 5% (B) and 9% (C) strain and comparison of dislocation slip lines' average density near and far from the grain boundary (D). SEM: Scanning electron microscopy; TZ: Ti-Zr-V-Nb-Al.

CONCLUSION

The refined non-equiatomic BCC Ti-Zr-V-Nb-Al HEA with a grain size of 15 μm was prepared in the present study. The alloy exhibits a superior combination of high yield strength (840 MPa) and large uniform elongation (12.0%). The increased density of grain boundaries promotes the uniformity of dislocation distribution. As the density of grain boundaries increased, the long-range propagation of the planar-slip

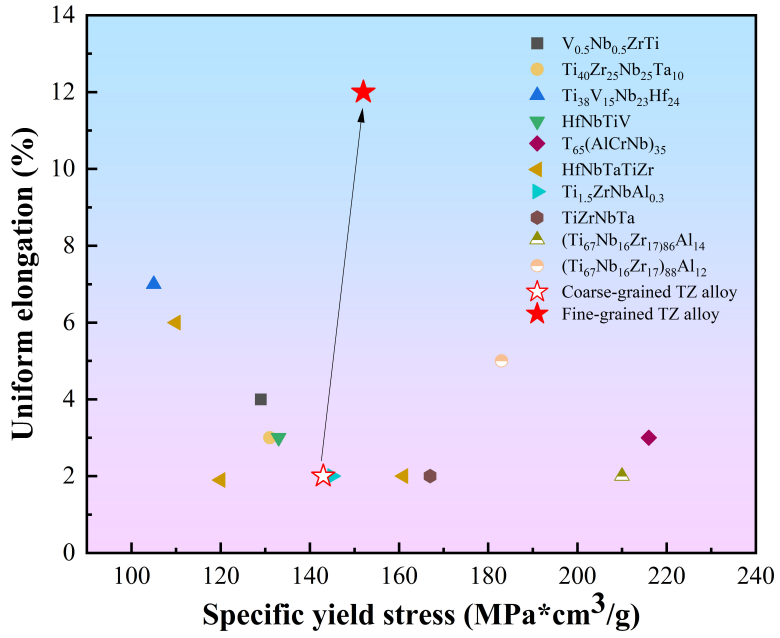

Figure 8. Specific yield strength vs. uniform elongation of TZ alloy compared with existing BCC HEAs[6-10,13,19,24-27]. TZ: Ti-Zr-V-Nb-Al; TZ: Ti-Zr-V-Nb-Al.

bands was effectively impeded. Meanwhile, a large number of dislocations are uniformly distributed along grain boundaries. During the alloy deformation process, dislocations are continuously entangled near the grain boundaries and the strengthening of the grain boundaries becomes more significant. Our results may provide a simple strategy for improving the uniform ductility of BCC HEAs, leading to their potential engineering applications.

DECLARATIONS

Authors' contributions

Data acquisition, analysis, and interpretation and writing of the first draft: Zeng, H.; Han, M.
Provided material, conception and design of the study and interpretation: Li, B.; Wang, B.; Wang, L.
Data analysis and interpretation and contribution to the development of the article: Wang, B.; Wang, L.; Jin, K.; Sun, S.; Xue Y.; Wang, L.

Availability of data and materials

Not applicable.

Financial support and postcode

This work was supported by the YEQISUN Joint Funds of the National Science Foundation of China (Grant No. U2241234), National Natural Science Foundation of China (Grant Nos. 52301127 and 52171028), and the Scientific Research Foundation for the Youth Scholars of Beijing Institute of Technology (Grant No. XSQD-202008003). The use of the APS at ANL was supported by the U.S. Department of Energy (Grant No. DE-AC02-06CH11357). The State Key Program of National Natural Science of China (Grant No. 12132003).

Conflicts of interest

All authors declared that there are no conflicts of interest.

Ethical approval and consent to participate

Not applicable.

Consent for publication

Not applicable.

REFERENCES

1. Edalati, P.; Mohammadi, A.; Ketabchi, M.; Edalati, K. Microstructure and microhardness of dual-phase high-entropy alloy by high-pressure torsion: twins and stacking faults in FCC and dislocations in BCC. *J. Alloys. Compd.* **2022**, *894*, 162413. DOI
2. Edalati, P.; Mohammadi, A.; Tang, Y.; Floriano, R.; Fuji, M.; Edalati, K. Phase transformation and microstructure evolution in ultrahard carbon-doped AlTiFeCoNi high-entropy alloy by high-pressure torsion. *Mater. Lett.* **2021**, *302*, 130368. DOI
3. Yeh, J.; Chen, S.; Lin, S.; et al. Nanostructured high-entropy alloys with multiple principal elements: novel alloy design concepts and outcomes. *Adv. Eng. Mater.* **2004**, *6*, 299-303. DOI
4. Edalati, P.; Mohammadi, A.; Ketabchi, M.; Edalati, K. Ultrahigh hardness in nanostructured dual-phase high-entropy alloy AlCrFeCoNiNb developed by high-pressure torsion. *J. Alloys. Compd.* **2021**, *884*, 161101. DOI
5. Kim, K.; Warren, P.; Cantor, B. Glass-forming ability of novel multicomponent $(Ti_{33}Zr_{33}Hf_{33})$-$(Ni_{50}Cu_{50})$-Al alloys developed by equiatomic substitution. *Mater. Sci. Eng. A.* **2004**, *375-377*, 317-21. DOI
6. An, Z.; Mao, S.; Yang, T.; et al. Spinodal-modulated solid solution delivers a strong and ductile refractory high-entropy alloy. *Mater. Horiz.* **2021**, *8*, 948-55. DOI
7. Liao, Y.; Li, T.; Tsai, P.; et al. Designing novel lightweight, high-strength and high-plasticity Ti*x*$(AlCrNb)_{100-x}$ medium-entropy alloys. *Intermetallics* **2020**, *117*, 106673. DOI
8. Senkov, O. N.; Pilchak, A. L.; Semiatin, S. L. Effect of cold deformation and annealing on the microstructure and tensile properties of a HfNbTaTiZr refractory high entropy alloy. *Metall. Mater. Trans. A.* **2018**, *49*, 2876-92. DOI
9. Pang, J.; Zhang, H.; Zhang, L.; et al. Ductile $Ti_{1.5}ZrNbAl_{0.3}$ refractory high entropy alloy with high specific strength. *Maters. Lett.* **2021**, *290*, 129428. DOI
10. Wang, S.; Ma, E.; Xu, J. New ternary equi-atomic refractory medium-entropy alloys with tensile ductility: Hafnium versus titanium into NbTa-based solution. *Intermetallics* **2019**, *107*, 15-23. DOI
11. Wang, L.; Chen, S.; li, B.; et al. Lightweight $Zr_{1.2}V_{0.8}NbTi_xAl_y$ high-entropy alloys with high tensile strength and ductility. *Mater. Sci. Eng. A.* **2021**, *814*, 141234. DOI
12. Lei, Z.; Liu, X.; Wu, Y.; et al. Enhanced strength and ductility in a high-entropy alloy via ordered oxygen complexes. *Nature* **2018**, *563*, 546-50. DOI
13. Lilensten, L.; Couzinié, J.; Perrière, L.; et al. Study of a bcc multi-principal element alloy: tensile and simple shear properties and underlying deformation mechanisms. *Acta. Mater.* **2018**, *142*, 131-41. DOI
14. Vystavěl, T.; Jacques, A.; Gemperle, A.; Gemperlová, J.; George, A. Dislocation interaction with a Σ=3 grain boundary observed by in situ TEM. *Mater. Sci. Forum.* **1998**, *294-6*,397-400. Available from: https://pascal-francis.inist.fr/vibad/index.php?action=getRecordDetail&idt=1576291. [Last accessed on 20 Jan 2025].
15. Cheng, S.; Spencer, J.; Milligan, W. Strength and tension/compression asymmetry in nanostructured and ultrafine-grain metals. *Acta. Mater.* **2003**, *51*, 4505-18. DOI
16. Horita, Z.; Smith, D. J.; Furukawa, M.; Nemoto, M.; Valiev, R. Z.; Langdon, T. G. An investigation of grain boundaries in submicrometer-grained Al-Mg solid solution alloys using high-resolution electron microscopy. *J. Mater. Res.* **1996**, *11*, 1880-90. DOI
17. Toby, B. H.; Von, D. R. B. *GSAS*-II: the genesis of a modern open-source all purpose crystallography software package. *J. Appl. Cryst.* **2013**, *46*, 544-9. DOI
18. Yi, H. L.; Chang, Z. Y.; Cai, H. L.; Du, P. J.; Yang, D. P. Strength, ductility and fracture strain of press-hardening steels. *Acta Metall. Sin.* **2020**, *56*, 429-43. Available from: https://www.ams.org.cn/EN/10.11900/0412.1961.2020.00003. [Last accessed on 20 Jan 2025].
19. Wu, Y.; Cai, Y.; Wang, T.; et al. A refractory $Hf_{25}Nb_{25}Ti_{25}Zr_{25}$ high-entropy alloy with excellent structural stability and tensile properties. *Maters. Letts.* **2014**, *130*, 277-80. DOI
20. Ungár, T.; Dragomir, I.; Révész, Á.; Borbély, A. The contrast factors of dislocations in cubic crystals: the dislocation model of strain anisotropy in practice. *J. Appl. Cryst.* **1999**, *32*, 992-1002. DOI
21. Lee, C.; Kim, G.; Chou, Y.; et al. Temperature dependence of elastic and plastic deformation behavior of a refractory high-entropy alloy. *Sci. Adv.* **2020**, 6. DOI PubMed PMC
22. Lee, C.; Maresca, F.; Feng, R.; et al. Strength can be controlled by edge dislocations in refractory high-entropy alloys. *Nat. Commun.* **2021**, *12*, 5474. DOI PubMed PMC
23. Dirras, G.; Gubicza, J.; Heczel, A.; et al. Microstructural investigation of plastically deformed $Ti_20Zr_{20}Hf_{20}Nb_{20}Ta_{20}$ high entropy alloy by X-ray diffraction and transmission electron microscopy. *Mater. Charact.* **2015**, *108*, 1-7. DOI

24. Chen, Y.; Xu, Z.; Wang, M.; Li, Y.; Wu, C.; Yang, Y. A single-phase $V_{0.5}Nb_{0.5}ZrTi$ refractory high-entropy alloy with outstanding tensile properties. *Mater. Sci. Eng. A.* **2020**, *792*, 139774. DOI
25. Nguyen, V.; Qian, M.; Shi, Z.; Song, T.; Huang, L.; Zou, J. Compositional design of strong and ductile (tensile) Ti-Zr-Nb-Ta medium entropy alloys (MEAs) using the atomic mismatch approach. *Mater. Sci. Eng. A.* **2019**, *742*, 762-72. DOI
26. Wei, S.; Kim, S. J.; Kang, J.; et al. Natural-mixing guided design of refractory high-entropy alloys with as-cast tensile ductility. *Nat. Mater.* **2020**, *19*, 1175-81. DOI
27. Zhang, Y.; Bu, Z.; Yao, T.; Yang, L.; Li, W.; Li, J. Novel BCC Ti-Al-Nb-Zr medium-entropy alloys with ultrahigh specific strength and ductility. *J. Alloys. and. Compd.* **2023**, *936*, 168290. DOI